WAFER-BONDED TWO-TERMINAL III-V//SI TRIPLE-JUNCTION SOLAR CELL WITH POWER CONVERSION EFFICIENCY OF 36.1 % AT AM1.5G

Patrick Schygulla[1], Ralph Müller[1], Oliver Höhn[1], Michael Schachtner[1], David Chojniak[1], Andrea Cordaro[2], Stefan Tabernig[2], Benedikt Bläsi[1], Albert Polman[2], Gerald Siefer[1], David Lackner[1], and Frank Dimroth[1]
[1]Fraunhofer Institute for Solar Energy Systems ISE, Freiburg, Germany
[2]NWO-Institute AMOLF, Amsterdam, The Netherlands
patrick.schygulla@ise.fraunhofer.de

ABSTRACT: In this work, we present the fabrication and analysis of a wafer-bonded GaInP/GaInAsP//Si triple-junction solar cell with 36.1 % conversion efficiency under AM1.5g spectral illumination. The new cell design presents an improvement over previous III-V//Si triple-junction cells by the implementation of a rear-heterojunction design for the middle cell. Furthermore, an advanced metallodielectric rear-side grating was used for light trapping enhancement in the silicon bottom cell that increased the silicon subcell current by 1.4 mA/cm². A luminescent coupling factor of 0.46 between the middle and bottom subcell was determined. The share of recombination in the middle cell space-charge region was experimentally shown to be insignificant as intended by the rear-heterojunction design. Overall, the open-circuit voltage increased by 61 mV compared to the previous generation. Given the established long-term stability of III-V and silicon based solar cells these results are promising steps towards the future employment of III-V/Si tandem solar cells.
Keywords: silicon-based tandem solar cell, III-V//Si, multi-junction, MOVPE, GaInAsP

1 INTRODUCTION

The record efficiency of silicon single-junction solar cells is close to its theoretical efficiency limit of 29.4 – 29.5 % [1,2]. Further increasing the cell efficiency [3] is an important driver for photovoltaics system cost reduction. Hence, there is the strong need for new solar cell concepts exceeding the silicon single-junction efficiency limit. Multi-junction solar cells are a promising concept to this end with demonstrated efficiencies of up to 39.5 % for a triple-junction cell fully made from III-V semiconductors [4]. Such cells are grown by epitaxial deposition on an expensive GaAs or InP substrate. Hence, we investigated the efficiency potential of III-V top structures combined with a silicon bottom cell to improve the efficiency-to-cost ratio.

Wafer-bonded III-V//Si multi-junction solar cells were the first monolithic silicon-based tandem cells to surpass a conversion efficiency of 30 %. In the past, we have shown further efficiency improvements by a) the inclusion of a TOPCon surface passivation of the silicon bottom cell together with integration of a diffractive light scattering structure on the rear side, reaching 33.3 % [5], b) the employment of an absorber material with a higher band gap in the second junction, AlGaAs instead of GaAs, reaching 34.1 % [6], and c) the employment of a material with higher minority carrier lifetimes, GaInAsP instead of AlGaAs, reaching 35.9 % [7].

Other promising tandem cell concepts involving silicon bottom cells are dual junctions employing a perovskite top cell. With this technology, the highest efficiencies exceed 30 % on a 1 cm² device [8]. Solar cells including perovskite absorbers exhibit degradation over time, for which a solution has not yet been found, though. [9]. Combining more than two junctions using perovskite absorbers is challenging due to wet-chemical processing issues and reduced availability of materials at the required higher band gaps. The highest efficiency for a monolithic triple-junction perovskite/perovskite/silicon device amounts to 20 % [10].

Here, we present a GaInP/GaInAsP//Si triple-junction solar cell with a further improved heterojunction structure of the III-V layer stack, combined with the previously demonstrated metallodielectric light trapping back-side reflector. We measured a conversion efficiency of 36.1%,

the highest value observed for a Si-based solar cell. The high efficiency enables a detailed study of the carrier collection quantum efficiency and spontaneous emission processes that determine the high efficiency.

2 METHODS

2.1 Epitaxial Growth

III-V semiconductor layers were epitaxially grown lattice matched to GaAs by metalorganic vapour phase epitaxy in a commercial AIX2800G4 reactor from AIXTRON. 4" (001)-oriented GaAs wafers with an offcut of 6 ° into the [111]-B direction were used as substrates. TMAl, TMGa, TMIn, AsH3, PH3, DMZn, and SiH4 were used as precursors. In both the middle and the top cell, a rear-heterojunction design was employed. The first reason for this choice is the higher minority carrier lifetime of n-GaInAsP, the only absorber material in the rear-heterojunction, compared to p-GaInAsP [11], the thickest part of the absorber in a homojunction. The second reason is the reduction of the dark current in the space charge region because of the increased band gap inside the space charge region at the rear-side of the absorber [12].

2.2 Solar Cell Processing

The middle cell was deposited first and the top cell second on the GaAs substrate to reduce the voltage drop in the top cell due to a high thermal load [7]. The upright growth fashion made it necessary to temporarily bond the epitaxial structure to a sapphire wafer as mechanical support. After that, the GaAs substrate was removed by wet chemical etching with citric acid. Then, the exposed bond layer was chemically mechanically polished by the company III/V-Reclaim. Next, a direct wafer bond to a TOPCon silicon cell was performed before the temporary bond could be released again by thermal slide at 190 °C. Solar cell processing involving photolithography, mesa etching, metal contact formation, and sputter deposition of an anti-reflection coating (ARC) followed. Twelve solar cells with a size of 2×2 cm² and a metal grid optimised for one-sun operation were processed on each wafer. After solar cell processing, the wafers were nano-imprinted with a diffractive grating on the rear side at AMOLF [13]. The rear-side grating is designed to enhance the optical path

length in the silicon bottom cell and thus increases Si subcell current. It is designed to minimize light scattering from the back-side reflector in normal direction and to enhance large-angle scattering in the Si cell, while minimizing parasitic absorption in the metal [14]. More details on the solar cell processing can be found in [5,7,15]. The final layer stack is shown in Figure 1.
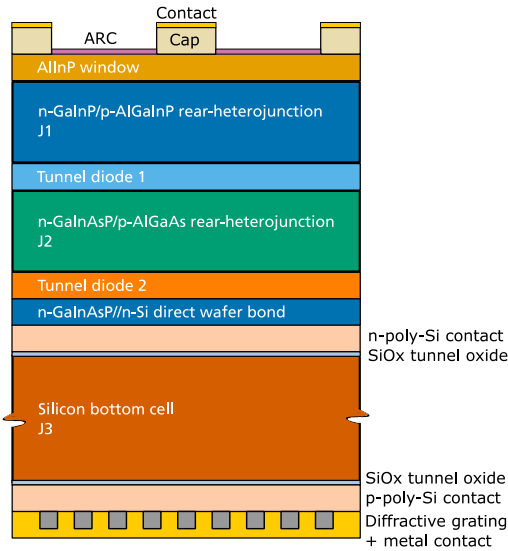

Figure 1. Layer stack of the III-V//Si triple-junction solar cell. The GaInP/GaInAsP top structure was attached to a TOPCon silicon bottom cell by surface-activated direct wafer bonding. The rear-side grating was implemented by nanoimprint lithography.

2.3 Characterisation

The solar cells were characterised by external quantum efficiency and current-voltage measurements before and after the diffractive rear-side grating was applied to evaluate the current gain. The *IV*-curves were recorded under calibrated spectral conditions of AM1.5g (IEC 60904-3:2019 (ed.4)) in the Fraunhofer ISE Calibration Laboratory (CalLab). Current-voltage characteristics were measured using a hard mask with an aperture area of 3.987 cm² , which is slightly lower than the mesa area of the solar cells, in order to prevent a lateral current contribution from the silicon bottom junction outside of the mesa area.

Additionally, the sub-cell currents were analysed under different spectral conditions to determine the luminescent coupling between sub-cells and the radiative recombination current of the top cells. For this advanced characterisation method, a Wavelabs SINUS 220 LED based solar simulator equipped with 20 spectrally different LED light sources was used [16]. Using the different LED channels the injection level on each subcell was varied in a systematic manner while the remaining subcells were light biased at AM1.5g conditions. A custom software was used to control the illumination unit of the solar simulator while the spectral adjustment of the individual light sources was realized using the procedure described in [17].

3 RESULTS

3.1 Current-Voltage Characteristics

The current champion solar cell has a power conversion efficiency of 36.1 % under the AM1.5g spectrum as was determined by a calibrated current-voltage measurement that is shown in Figure 2. The main reason for the higher efficiency compared to the last generation of III-V//Si triple-junction solar cells made at Fraunhofer ISE is the increase in open-circuit voltage by 61 mV. The major difference compared to the previous generation is the inclusion of a rear-heterojunction cell configuration in place of the former homojunction cell design for the middle cell.
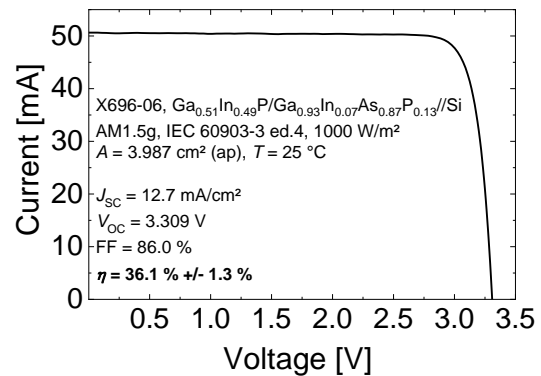

Figure 2. Current-voltage characteristics of the champion GaInP/GaInAsP//Si triple-junction solar cell measured in the Fraunhofer ISE CalLab under a calibrated AM1.5g spectrum.

3.2 External Quantum Efficiency

The external quantum efficiency (EQE) of the champion cell X696-6 is shown in Figure 3. The subcell current density is calculated from the injection current variation experiments explained below. That analysis shows that the middle cell is current limiting with 12.6 mA/cm². The sum of the subcell currents amounts to 38.9 mA/cm² which implies current matched conditions at a jsc of around 13.0 mA/cm² at the currently prevailing optical and electrical performance. Thus, the middle cell is limiting by 0.4 mA/cm². The difference of 0.1 mA/cm² in the short-circuit current density of the entire triple-junction, 12.7 mA/cm², compared to the subcell current density of the middle cell, 12.6 mA/cm², is caused by two effects. The first effect is luminescence coupling from the top to the middle cell. Considering the difference in subcell current between the top and middle cell, 0.6 mA/cm², this implies that around a fifth to a quarter of the excessively injected charge carriers recombine radiatively in the top cell and these photons are then reabsorbed in the middle cell. The second effect is a small decrease in current density from $V = 0$ towards the short-circuit point of the current limiting subcell, at $V = V_{oc} - V_{oc,j2}$ due to a finite parallel resistance.

Before the nanoimprint of the diffractive rear-side structure the short-circuit current density was limited by the silicon bottom cell with 11.7 mA/cm². Hence, the light path enhancement that leads to increased absorption in the long-wavelength regime close to the absorption threshold for silicon, around 1100 nm, resulted in an increase in current density by 1.4 mA/cm² to a total value of 13.1 mA/cm². Differently designed versions of a rear-side diffractive structure in previous experiments lead to a current density gain of 1.1 mA/cm² in the silicon bottom

cell [18].

If the subcell currents of a multi-junction solar cell are perfectly matched, then the rounding of the individual IV-curves at the maximum power point adds up and the fill factor of the IV-curve of the entire device is reduced. Conversely, in strong current-mismatched conditions the fill factor is dominated by the fill factor of the current limiting subcell [19]. If the available solar resource was distributed more evenly between all subcells, while maintaining the material quality and thus the open-circuit voltage, the power conversion efficiency could still be improved by 0.4 %$_{abs}$ to 36.5 % with mere adjustments to the absorber thicknesses.
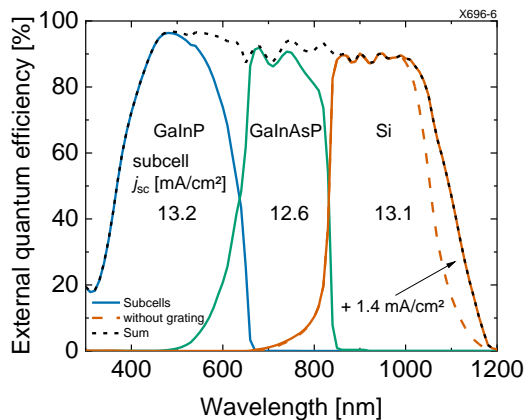

Figure 3. External quantum efficiency of the three subcells (solid line) and of the entire triple-junction solar cell (black, dotted line). The quantum efficiency of the silicon bottom cell before the imprint of the diffractive rear-side grating is shown by the orange dashed line.

3.3 Luminescence Coupling

The high amount of radiative recombination in the middle cell results in luminescence coupling from the second to the third junction. Photons that are emitted after radiative recombination of charge carriers in the middle cell have a certain probability of leaving the junction towards the bottom and be reabsorbed by the bottom cell. If the bottom cell limits the overall current, then this luminescent contribution increases the short-circuit current. Following the procedure suggested by Steiner et al. [20], the irradiance of each subcell was systematically decreased and increased with respect to AM1.5g 1-sun conditions while the other subcells were biased with light to maintain an AM1.5g injection level. The measured short-circuit currents for the different irradiance conditions are shown in Figure 4.

On the left side of the diagram where the slopes are constant, the subcell for which the photocurrent is varied is current limiting in each case. The second junction is current limiting at 1 sun. This is why the photocurrent of the second junction must be increased above 1 sun to reach current matching with the top cell at 13.2 mA/cm². Then, the top cell becomes limiting and the overall current stagnates. For the first junction, one can see that upon further increase of the photocurrent beyond 0.96 suns the overall current increases again due to luminescent coupling from the first to the second junction with the coupling factor η_{12}. If the irradiance of the third junction is decreased below around 0.97 suns, then that junction becomes limiting. From the curve shape of the injection variation of the bottom cell the luminescence coupling

factor η_{23} from the second to the third junction can be extracted. The second junction is optically thick for light emitted by the first junction so the contribution of coupled light from the first directly to the third junction can be neglected.
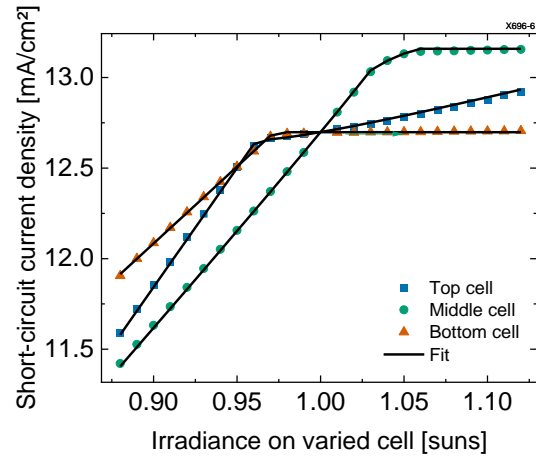

Figure 4. Measured short-circuit current of the III-V//Si 3j champion device upon selective variation of the photocurrent in the top (blue squares), middle (cyan circles), and bottom junction (orange triangles) around AM1.5g conditions at 1 sun. The other junctions are biased at the 1-sun conditions, respectively. The fitted curves to the data are shown by solid black lines.

4   CONCLUSIONS

We present a III-V//Si triple-junction solar cell with a GaInP top cell, a GaInAsP middle cell, and a silicon bottom cell with a conversion efficiency of 36.1 %, the highest efficiency reported for a Si-based multi-junction solar cell reported to date. The III-V top cell structure was wafer-bonded to the silicon bottom cell for a monolithic integration. A metallodielectric back-side reflector was integrated to optimize light trapping in the Si bottom cell. By employing a rear-heterojunction cell design in both the middle and top cell, the open-circuit voltage of the triple-junction device could be improved by 61 mV compared to previous generations. Since radiative recombination of minority carriers is dominant in this structure strong luminescent coupling between the middle and bottom subcell was observed. This was carefully considered for accurate quantification of the external quantum efficiency. An absolute determination of the external quantum efficiencies of every subcell was important for evaluating the current gain caused by the back-side reflector. Acquiring current-voltage curves at systematically varying irradiance conditions selectively for each subcell is a useful method for obtaining the luminescence coupling factors and the externally injected currents for calibration of the external quantum efficiency.

References

1. Richter A, Hermle M, Glunz SW. Reassessment of the Limiting Efficiency for Crystalline Silicon Solar Cells. *IEEE J. Photovolt.* 2013; **3(4)**: 1184–91, DOI: 10.1109/JPHOTOV.2013.2270351.
2. Veith-Wolf BA, Schäfer S, Brendel R, Schmidt J. Reassessment of intrinsic lifetime limit in n-type crystalline silicon and implication on maximum solar cell efficiency. *Sol. Energy Mater. Sol. Cells* 2018; **186**: 194–9, DOI: 10.1016/j.solmat.2018.06.029.
3. Benda V, Černá L. PV cells and modules - State of the art, limits and trends. *Heliyon* 2020; **6(12)**: e05666, DOI: 10.1016/j.heliyon.2020.e05666.
4. France RM, Geisz JF, Song T, Olavarria W, Young M, Kibbler A, Steiner MA. Triple-junction solar cells with 39.5% terrestrial and 34.2% space efficiency enabled by thick quantum well superlattices. *Joule* 2022; **6(5)**: 1121–35, DOI: 10.1016/j.joule.2022.04.024.
5. Cariou R, Benick J, Feldmann F, Höhn O, Hauser H, Beutel P, Razek N, Wimplinger M, Bläsi B, Lackner D, Hermle M, Siefer G, Glunz SW, Bett AW, Dimroth F. III–V-on-silicon solar cells reaching 33% photoconversion efficiency in two-terminal configuration. *Nat. Energy.* 2018; **3(4)**: 326–33, DOI: 10.1038/s41560-018-0125-0.
6. Lackner D, Höhn O, Müller R, Beutel P, Schygulla P, Hauser H, Predan F, Siefer G, Schachtner M, Schön J, Benick J, Hermle M, Dimroth F. Two-Terminal Direct Wafer-Bonded GaInP/AlGaAs//Si Triple-Junction Solar Cell with AM1.5g Efficiency of 34.1%. *Sol. RRL* 2020; **4(9)**: 2000210, DOI: 10.1002/solr.202000210.
7. Schygulla P, Müller R, Lackner D, Höhn O, Hauser H, Bläsi B, Predan F, Benick J, Hermle M, Glunz SW, Dimroth F. Two-terminal III–V//Si triple-junction solar cell with power conversion efficiency of 35.9 % at AM1.5g. *Prog Photovolt Res Appl.* 2022; **30(8)**: 869–79, DOI: 10.1002/pip.3503.
8. Green MA, Dunlop ED, Siefer G, Yoshita M, Kopidakis N, Bothe K, Hao X. Solar cell efficiency tables (Version 61). *Prog Photovolt Res Appl.* 2023; **31(1)**: 3–16, DOI: 10.1002/pip.3646.
9. Tockhorn P, Sutter J, Cruz A, Wagner P, Jäger K, Yoo D, Lang F, Grischek M, Li B, Li J, Shargaieva O, Unger E, Al-Ashouri A, Köhnen E, Stolterfoht M, Neher D, Schlatmann R, Rech B, Stannowski B, Albrecht S, Becker C. Nano-optical designs for high-efficiency monolithic perovskite-silicon tandem solar cells. *Nat. Nanotechnol.* 2022; **17(11)**: 1214–21, DOI: 10.1038/s41565-022-01228-8.
10. Zheng J, Wang G, Duan W, Mahmud MA, Yi H, Xu C, Lambertz A, Bremner S, Ding K, Huang S, Ho-Baillie AWY. Monolithic Perovskite–Perovskite–Silicon Triple-Junction Tandem Solar Cell with an Efficiency of over 20%. *ACS Energy Lett.* 2022; **7(9)**: 3003–5, DOI: 10.1021/acsenergylett.2c01556.
11. Schygulla P, Heinz FD, Dimroth F, Lackner D. Middle Cell Development for Wafer-Bonded III-V//Si Tandem Solar Cells. *IEEE J. Photovolt.* 2021; **11(5)**: 1264–70, DOI: 10.1109/JPHOTOV.2021.3090159.
12. Hwang S-T, Kim S, Cheun H, Lee H, Lee B, Hwang T, Lee S, Yoon W, Lee H-M, Park B. Bandgap grading and Al0.3Ga0.7As heterojunction emitter for highly efficient GaAs-based solar cells. *Sol. Energy Mater. Sol. Cells* 2016; **155**: 264–72, DOI: 10.1016/j.solmat.2016.06.009.
13. Cordaro CEA, Tucher N, Tabernig S, Hauser H, Höhn O, Müller R, Bläsi B, Polman A. Plasmonic and Mie scattering in nanopatterned back reflectors for III–V-on-silicon solar cells (Conference Presentation). In: Sprafke A, Goldschmidt JC, Pandraud G, (eds). *Photonics for Solar Energy Systems VIII: 6-10 April 2020, online only, France*. Bellingham, Washington, USA: SPIE; 2020, p. 1136607.
14. Cordaro A, Müller R, Tabernig S, Tucher N, Schygulla P, Höhn O, Bläsi B, Polman A. *Nano-patterned back-reflector with engineered near-field/far-field light scattering for enhanced light trapping in silicon-based multi-junction solar cells*; 2023.
15. Müller R, Schygulla P, Lackner D, Höhn O, Hauser H, Richter A, Fell A, Bläsi B, Predan F, Benick J, Hermle M, Dimroth F, Glunz SW. Silicon-Based Monolithic Triple-Junction Solar Cells with Conversion Efficiency >34%. In: *37th European Photovoltaic Solar Energy Conference and Exhibition*. Proceedings; 2020, pp. 574–578.
16. Scherff MLD, Nutter J, Fuss-Kailuweit P, Suthues J, Brammer T. Spectral mismatch and solar simulator quality factor in advanced LED solar simulators. *Jpn. J. Appl. Phys.* 2017; **56(8S2)**: 08MB24, DOI: 10.7567/jjap.56.08mb24.
17. Chojniak D, Bett AJ, Hohl-Ebinger J, Reichmuth SK, Schachtner M, Siefer G. LED solar simulators – A spectral adjustment procedure for tandem solar cells. *AIP Conf. Proc.* 2023; **2826(1)**: 30003, DOI: 10.1063/5.0140990.
18. Bläsi B, Höhn O, Hauser H, Cariou R, Benick J, Feldmann F, Beutel P, Lackner D, Hermle M, Siefer G, Glunz SW, Bett AW, Dimroth F, Tucher N. Photonic structures for III-V//Si multijunction solar cells with efficiency >33%. In: Wehrspohn RB, Sprafke AN, (eds). *Photonics for Solar Energy Systems VII*: SPIE; 2018, p. 2.
19. McMahon WE, Emery KE, Friedman DJ, Ottoson L, Young MS, Ward JS, Kramer CM, Duda A, Kurtz S. Fill factor as a probe of current-matching for GaInP 2 /GaAs tandem cells in a concentrator system during outdoor operation. *Prog Photovolt Res Appl.* 2008; **16(3)**: 213–24, DOI: 10.1002/pip.798.

20. Steiner M, Geisz JF, Moriarty TE, France RM, McMahon WE, Olson JM, Kurtz SR, Friedman DJ. Measuring *IV* curves and subcell photocurrents in the presence of luminescent coupling. *IEEE J. Photovolt.* 2013; **3(2)**: 879–87, DOI: 10.1109/jphotov.2012.2228298.